STADIUS
Center for Dynamical Systems, Signal Processing and Data Analytics

Citation/Reference	M. Lavanga et al., "**An autonomic age model for premature infants : a bradycardia perspective**," *Submitt. to Trans. Biomed. Eng.*, 2020.
Archived version	Author manuscript: the content is identical to the content of the published paper, but without the final typesetting by the publisher
Published version	Submitted
Journal homepage	https://www.embs.org/tbme/
Author contact	your email mlavanga@esat.kuleuven.be your phone number +32 16 37 38 28
Abstract	Objective: The development of premature infants has been described by means of EEG and fMRI, but few studies have focused on the autonomic nervous system (ANS) maturation. The aim of this study was to provide a normative maturation chart for premature infants based on heart-rate variability. Methods: ECG data were measured for at least 3 hours in 25 preterm infants (gestational age ≤ 32 weeks). After deriving the RR interval time-series, the signal was segmented based on heart-rate drop events, called bradycardias. Specifi- cally, different temporal, spectral and temporal features were extracted in the period after bradycardias (post-bradycardia), in the period between bradycardias and the period during each bradycardia. Different linear-mixed effect models were developed to estimate the post-menstrual age of the patients. Results: The models to estimate the age via HRV indices can have performance up to R2 = 0.78 and mean absolute error MAE = 1.74 weeks, but the best performance is reached if bradycardias are take into account. Conclusions: Three main novelties can be reported. First, the obtained autonomic- age models are comparable to EEG-based maturation models. Second, the selected subset of features for age prediction show a predominance of power features in the very-low and low frequency bands and higher scale fractal indices in explaining the infants'sympatho-vagal development. Third, bradycardias might disrupt the relationship between autonomic indices and age. Significance: Eventually, this approach might give a better overview in the

	investigation of postnatal maturation of pre- mature infants and tune neonatal care to improve patients' outcome..
IR	

(article begins on next page)

An autonomic age model for premature infants: a bradycardia perspective

M Lavanga*,1, E R M Heremans*,1, J Moeyersons[1], B Bollen[3]
K Jansen[3,4], E Ortibus[3], S Van Huffel[1], G Naulaers[3], A Caicedo[2]

***Abstract*— *Objective*: The development of premature infants has been described by means of EEG and fMRI, but few studies have focused on the autonomic nervous system (ANS) maturation. The aim of this study was to provide a normative maturation chart for premature infants based on heart-rate variability. *Methods*: ECG data were measured for at least 3 hours in 25 preterm infants (gestational age ≤ 32 weeks). After deriving the RR interval time-series, the signal was segmented based on heart-rate drop events, called *bradycardias*. Specifically, different temporal, spectral and temporal features were extracted in the period after bradycardias (post-bradycardia), in the period between bradycardias and the period during each bradycardia. Different linear-mixed effect models were developed to estimate the post-menstrual age of the patients. *Results*: The models to estimate the age via HRV indices can have performance up to $R^2 = 0.78$ and mean absolute error $MAE = 1.74\ weeks$, but the best performance is reached if bradycardias are take into account. *Conclusions*: Three main novelties can be reported. First, the obtained autonomic-age models are comparable to EEG-based maturation models. Second, the selected subset of features for age prediction show a predominance of power features in the very-low and low frequency bands and higher scale fractal indices in explaining the infants'sympatho-vagal development. Third, bradycardias might disrupt the relationship between autonomic indices and age. *Significance*: Eventually, this approach might give a better overview in the investigation of postnatal maturation of premature infants and tune neonatal care to improve patients' outcome.**

I. Introduction

Premature infants represent 10% of the neonatal population and are at higher risk for development disorders that can lead to adverse outcome [3]. The investigation of maturation via multiple physiological biomarkers is part of the clinical practice to limit the effect of outcomes later on in life [15], [7], [9]. The development of the neurovegetative functions or *Autonomic Nervous System* (ANS) can be described via the heart-rate fluctuations, known as *Heart-rate variability* (HRV).

Although the autonomic functions mature in both fetuses and premature infants, the preterm HRV is usually characterized by a lower vagal-tone due to the exposure to the ex-utero environment. This aberrant sympathetic response tends to diminish with development [14],[26]. Due to the rapid maturation of infants and the dismaturity effect due to early-life experiences, the fetal and preterm HRV frequency bands are still subject of an intensive discussion in the literature. In adults, the contribution of the sympathetic branch of the ANS is usually represented by the low-frequency band (LF, $[0.04 - 0.15]\ Hz$) of the HRV, while the high-frequency band (HF, $[0.15 - 0.5]\ Hz$) reflects the stimulation of the parasympathetic branch. The very-low frequency band (VLF, $[0 - 0.04]\ Hz$) is usually associated to thermal and hormonal regulation, while the sympathovagal balance can be expressed by the power ratio of the two frequency bands $\left(\frac{LF}{HF}\right)$. However, Doret [8] and David [5] questioned the traditional frequency bands definition for the HRV short-term analysis in fetal heart-rate. In particular, they concluded that the presence of a "two-bumps" spectrum behavior with infant's heart-rate has not been demonstrated yet and new ways to investigate the sympathovagal balance should be defined. This could explain why Krueger [17] didn't find any specific change in a $\frac{LF}{HF}$ ratio longitudinal study with preterm patients, while Hoyer [12] was able to describe brain maturation by means of the fetal autonomic brain age score (FABAS), which was comprised of $\frac{VLF}{LF}$ as sympathovagal balance. In particular, Hoyer [12] interestingly argues that the predominant principles of development are increasing fluctuation amplitude, increasing complexity and pattern formation. Consequently, HRV indices can be chosen to reflect these principles in order to describe autonomic maturation.

However, it should not be forgotten that premature infants also experience bradycardias and apneas as common events. These may alter oxygen saturation and blood flow putting organs at risk of damage [23]. In general, apneas and bradycardias can be uncorrelated, but apneic spells that occur with bradycardias are most likely to affect brain homeostasis. In addition, apneas and bradycardias are the probable consequence of the immature respiratory system and the apneas' occurrence tends to decrease with infants' development [2] [25]. Bradycardia can then be considered consequence of heart-rate disregulation. Therefore, a proper maturation model that is based on HRV should also include the possible effect of those events in any statistical feature derived by the HRV.

In order to address the shortcomings by the studies outlined above, a new framework to describe autonomic maturation in healthy preterm babies has been provided. This research can

* Joint first authors
[1] Department of Electrical Engineering (ESAT), STADIUS Center for Dynamical Systems, Signal Processing and Data Analytics, KU Leuven, Belgium mlavanga at esat.kuleuven.be
[2]Department of Applied Mathematics and Computer Science, Faculty of Natural Sciences and Mathematics, Universidad del Rosario, Bogotá, Colombia
[3]Department of Development and Regeneration, Neonatal Intensive Care Unit, UZ Leuven, Belgium
[4]Department of Development and Regeneration, Child Neurology, UZ Leuven, Belgium

be divided in two main strands. First, both spectral analysis and multifractal analysis have been employed to investigate the neurovegetative development of the sympathovagal balance and its complexity and track maturation [8],[12]. Second, the impact of bradycardias on the description of ANS maturation and its quantification have been investigated. Up to our knowledge, this is the first study which tries to provide a complete overview of autonomic maturation in premature neonates, including non-stationary events such as bradycardias.

The final clinical objective is to provide normative maturation charts, that can be used as reference for stress-impact or ex-utero-impact studies and define suitable therapies in the neonatal intensive care unit. The paper is organized as follows: in section II, we introduce the dataset used for the study and the methods used to estimate and track the sympathovagal maturation. Section III reports the results, while section IV includes our discussion on the reported results.

II. Methods

A. Dataset

The dataset consists of 25 preterm infants (gestational age - GA ≤ 32 weeks), that were recruited for a larger study to assess brain development and design a sleep stage classifier at the Neonatal Intensive Care Unit of the University Hospital of Leuven, Belgium [7], [16]. All the patients were recorded with informed parental consent and presented normal development outcome at 2 years from birth. Data were recorded with 9 electrodes for the electroencephalogram (EEG) and with 3-leads for electrocardiogram (ECG) measurements. The sampling frequency was 250 or 500 Hz. On each patient, the measurements were performed at least twice. This results in a total of 74 recordings lasting 4h 55min on average. The post-menstrual ages (PMA) range from 28 weeks to 42 weeks.

B. Preprocessing

The heart rate variability (HRV) represents the instantaneous fluctuations of heart rate and is usually expressed by the tachogram which visualizes the variations of the time interval between two consecutive R-peaks (RR intervals, RR_i). In order to compute a RR_i time series, R peaks have been detected via the Matlab toolbox by Moeyersons et al. [21], which is based on the Pan-Tompkins algorithm. However, multiple artefacts can affect the R-peak detection process. In particular, missing R-peaks and large movement artefacts were present in the dataset. For the first type, the missing R-peak was replaced by linear correlation according to the formula:

$$\hat{R}_t = \frac{R_{t-1} + R_{t+1}}{2}, \tag{1}$$

where $\hat{R}_t$ is the estimated position of the missed R-peak, while R_{t-1} and R_{t+1} are the location of the previous and following R-peak. In case of large movement artifacts, the contaminated parts of the signal were discarded, but at least 1h of continuous signal was kept. Eventually, some recordings were completely discarded whenever less than 20 minutes of artifact-free data were available. Consequently, the total number of analyzed time series were 74.

Besides the preprocessing of artifacts, it is important to remember that premature infants can undergo bradycardias, which are sudden drops of heart-rate. Although those phenomena are completely natural in the developing infant, they can suddenly increase the frequency content of the RR_i series. Therefore, traditional linear spectral and temporal analysis might not be suitable since the instantaneous variance and mean of the heart-rate can vary over time, as explained in detail by [10]. According to Gee, the heart-rate activity that precedes sudden drops might differ from the drops itself and other bradycardia-free periods. As mentioned earlier, bradycardias can be a sign of immaturity of the cardiorespiratory control (rather than a parasympathetic stimulation) and different speculations have been made about the sources or the conditions that can have bradycardias as secondary effect [2]. Consequently, bradycardias have been detected in the current studies before any further processing. Based on the definitions of apnea of prematurity and bradycardias by [23], the bradycardia spells were detected as sudden RR_i increases above 1.5*$\overline{RR_i}$ that persist for more than 4 secs, where $\overline{RR_i}$ is the average tachogram. Subsequently, three different windowing strategies were applied:

1) Post-bradycardia windowing: the immediate 10 minutes after the bradycardic event were considered a candidate for features' extraction. It is important to remember this window did not include the bradycardia itself.
2) Between-bradycardias windowing: all non-overlapping 10 minute windows contained between bradycardic events were considered as candidate epochs for features' extraction. The first viable window was at least 10 minutes away from the bradycardic event in order to guarantee that the signal was stabilized.
3) Within-bradycardia windowing: a 10 minute window was considered from the moment that the signal reaches the threshold 1.5*$\overline{RR_i}$ in the tachogram, i.e. the supposed start of the bradycardic event. This windowing should involve both the information related to the heart-rate drop and the recovery period.

C. Temporal and spectral analysis

The first indices that have been computed to assess changes in HRV were the first and the second order moments of the RRi, i.e. the mean of the tachogram (μ_{RR}) and the standard deviation (σ_{RR}), as shown by [14]. However, in order to assess the sympathovagal activity, it is necessary to assess the power in different HRV frequency bands. In general, the RR time series is not stationary in any considered epoch, which could require time-frequency (TF) analysis to describe the oscillation shifts in the signal. Therefore, the HRV power spectral density (PSD) was estimated with Welch's periodogram as well as with time-frequency approaches, such as the quadratic smoothed pseudo Wigner-

Ville distribution (SPWD) [22] and the continuous wavelet transform [5]. Given a window size, Welch's algorithm estimates multiple periodograms in overlapping subwindows and averages them. On the other hand, the time-frequency approaches estimate the instantaneous autospectrum S_{xx} of the signal $x(t)$ (which is the RRi series). In case of SPWD, S_{xx} is estimated as follows:

$$S_{xx}(t,f) = \int\int_{-\infty}^{+\infty} \Phi_{xx}(\tau,\nu) A_{xx}(\tau,\nu) e^{j2\pi(t\nu-\tau f)} d\tau d\nu, \tag{2}$$

where $A_{xx}(\tau,\nu)$ is the ambiguity function, which is defined as the Fourier Transform of the time-dependent autocorrelation of $x(t)$ as follows

$$A_{xx}(\tau,\nu) = \int_{-\infty}^{+\infty} x(t+\tau/2)x^*(t-\tau/2)e^{-j2\pi t\nu} dt, \tag{3}$$

The smoothing of the time-frequency cross-coupling in Eq. 2 is done via the exponential kernel in the ambiguity domain defined as

$$\Phi_{xx}(\tau,\nu) = \exp\left\{ -\pi\left[\left(\frac{\nu}{\nu_0}\right)^2 + \left(\frac{\tau}{\tau_0}\right)^2\right]^{2\lambda}\right\}, \tag{4}$$

Following the study by [28], ν_0, τ_0, λ were set to 0.050, 0.046, and 0.3, respectively, leading to a kernel function with a TF resolution of [Δt, Δf] = [10.9 s, 0.03 Hz]. Similarly, $S_{xx}(t,f)$ can be computed as the scalogram of the wavelet transform of the signal as follows:

$$W_{xx}(t,s) = \int_{-\infty}^{+\infty} x(\tau)\psi^*\left(\frac{t-\tau}{s}\right) d\tau, \tag{5}$$

$$S_{xx}(t,f) = |W_{xx}(t,f)|^2, \tag{6}$$

where ψ is the mother wavelet (Analytic Morlet), while s stands for the scale of the wavelet transform and, in the general, $s \approx f^{-1}$.

Based on the given methodologies, the instantaneous power in the $\beta = [f_1, f_2]$ band of interest can be obtained as

$$P_\beta(t) = \int_{f1}^{f2} S_{xx}(t,f) df. \tag{7}$$

D. Multifractal analysis

Multifractal signals can be decomposed into different subsets characterized by local Hurst exponents h, which measure the regularities of the signal [13]. Small values of h represent sharp and transient regularity or singularity, while large values represent smooth changes [20]. Similarly to monofractal signals, it is possible to quantify the distribution of the embedding dimensions associated to each value of h. This function $D(h)$ is called the *singularity spectrum* (SS) and its determination is pivotal to assess the amount of singularities in the signal. A possible way to estimate the SS is the multifractal formalism based on the wavelet transform modulus maxima. Let $\psi_0(t)$ be a mother wavelet with a positive number of vanishing moments. The discrete wavelet transform (DWT) is defined by the inner product $d_{j,k} = \int_{\mathbb{R}} x(t)\psi_{j,k}(t)dt$, which decomposes $x(t)$ into elementary time-frequency components by means of translation $2^j k$ and dilation 2^j of the mother wavelet [27], since $\{\psi_{j,k}(t) = 2^{-j}\psi_0(2^j t - k), j \in \mathbb{R}, k \in \mathbb{R}\}$. Large scales describe smooth and low frequency oscillations, while small scales describe the sharp transitions in the signal. According to [27] and [24], a partition function $Z(2^j, q)$ can be estimated using the *wavelet leader* $L_f(j,k)$, as follows:

$$Z_L(2^j, q) = \frac{1}{n_k}\sum_{k=1}^{n_k} |L_f(j,k)|^q \sim 2^{j\tau(q)}, \tag{8}$$

where $L_f(j,k) \equiv L_\lambda$ represents the maximum wavelet coefficient in the narrow time neighborhood 3λ. Let $\lambda \equiv \lambda_{j,k} \equiv [k2^j, (k+1)2^j)$ be a dyadic interval, such that $d_\lambda = d_f(j,k)$ and let $3\lambda \equiv \lambda_{j,k-1} \cup \lambda_{j,k} \cup \lambda_{j,k+1}$ the union of three dyadic intervals, the wavelet leader is then defined as:

$$L_f(j,k) \equiv L_\lambda = \sup_{\lambda' \subset 3\lambda} \{|d_{\lambda'}|\}, \tag{9}$$

For certain values of q, the scaling exponent $\tau(q)$ (SE) has specific meaning: for positive respectively negative q, $Z(a,q)$ reflects scaling of large respectively short fluctuations. In general, for each q, the partition function exhibits a power-law decay characteristic, such as the power spectrum of 1/f noise. The scaling exponents (SE) associated to this decay can be obtained by computing the slope of Z versus the scales in a log-log diagram. Formally, the function $\tau(q)$ is estimated as follows:

$$\tau(q) = \lim_{j\to 0} \inf\left(\frac{log_2(Z_L(2^j,q))}{j}\right), \tag{10}$$

In case of a monofractal signal, $\tau(q)$ is a linear function $\tau(q) = qH - 1$, where H is the global Hurst exponent. In case of a multifractal signal, $\tau(q)$ is a nonlinear function of the local exponents h through the SS, as expressed by $\tau(q) = qh - D(h)$. Indeed, $D(h)$ can be written as the Legendre transform of $\tau(q)$, as follows $D(h) = qh - \tau(q)$ where $h = \frac{d\tau(q)}{dq}$. Since $\tau(q)$ can be decomposed using a Taylor expansion, $\tau(q) = \sum_{p=1}^{\infty} c_p \frac{q^p}{p!}$, SS can be rephrased in terms of the cumulants or coefficients c_p. For this study, we focused only on c_1 and c_2, which can be associated to the location of the maximum and the width of the $D(h)$ distribution. The parameter c_1 represents the main Hurst exponent of the signal, which will be referred to as H_{exp} from now on.

E. Algorithmic pipeline

All the methods above were used to extract a set of features useful to predict the ANS maturation in the preterm infants and a complete overview is reported in Table I. Before any processing, the RR_i signal was resampled at different sampling frequencies since the behavior of nonlinear features can depend on the sample rate of the tachogram [4]. The following sampling frequencies were

tested for fractal indices: [4,6,8,10,12,20] Hz. In contrast, the sampling frequencies 4 and 6 Hz were the only ones investigated for the spectral and temporal indices. Each signal was then split according to the three different windowing schemes mentioned above: Post-bradycardia windowing, Between-bradycardia windowing and Within-bradycardia windowing. In each non-overlapping window, the temporal, spectral and fractal features were then extracted.

Specifically, for the spectral analysis, tuning parameters were chosen in accordance to HRV task force [11], in order to assess the very low-frequency oscillations. In case of Welch's periodogram, the signal was further split in 50 % overlapping 3 minute windows. In case of SPWD, the parameters ν_0, τ_0 ,λ were set to 0.050, 0.046, and 0.3. The contributions of the different ANS branches were then assessed in terms of absolute and relative power in the following frequency bands, the very low-frequency VLF = $[0.0, 0.08]$ Hz, the low-frequency LF = $[0.08, 0.2]$ Hz and high frequency HF = $[0.2, 3.0]$ Hz [5]. The absolute power was actually assessed in the three bands, while the relative power was investigated as $\frac{VLF}{LF}$ and $\frac{LF}{HF}$ ratios and the normalized LF power as $\frac{LF}{VLF+LF}$ and $\frac{LF}{HF+LF}$. While Welch's method provides only one scalar value, the SPWD and the wavelet approaches generate a time series of the selected power band in the chosen time window. In order to obtain one value per window, the median of this time series was taken in account.

The multifractality parameters (c_1, c_2) were computed in the entire non-overlapping window. However, the chosen scale range $[j_1, j_2]$ of the *wavelet leader* transform can affect the computation of c_1 and c_2 [27]. Therefore, the set of parameters was derived according to the two ranges: $[j_1, j_2] = [3, 12]$ and $[j_1, j_2] = [5, 12]$. The former is the default range which should represent the entire HRV band [1], while the latter has been chosen to focus on the lower-frequency bands (i.e. VLF and LF) of the signal.

The features obtained for the different windowing schemes were then averaged throughout all epochs in order to get a representative value for each windowing scheme, i.e. one set of spectral, temporal and fractal indices for each phase (post-bradycardia, within-bradycardia and between bradycardias) and each patient. Therefore, after the features' extraction process, four datasets in three different conditions were extracted. The four datasets represent different subsets of features extracted form the recordings, in particular the spectral attributes, the temporal attributes, fractal indices and the combination of all three, while the three different conditions represent the three windowing schemes. The number of features extracted for the datasets are respectively: 21 for the spectral attributes, 2 for the temporal ones, 4 for fractal indices and 28 features in total.

In order to investigate the ANS maturation, the HRV features were used to predict the age of the patient. Since the post-menstrual age (PMA) is known for each recording, a regression model has been developed with PMA as response variable. The trend for the ANS features throughout the patients' development was reported as median(IQR) (where IQR stands for *InterQuartile Range*) in three age groups (PMA $\leq$ 31 weeks, PMA $\in (31 - 36]$ weeks, PMA $>$ 36 weeks) as well as Pearson correlation coefficient with PMA. The actual predictive power of the different sets of features were tested with a linear mixed-effect model [19]. First, the features were selected via the least absolute shrinkage and selection operator (LASSO). In particular, the LASSO reduction process was run 20 times on the entire dataset and only the features which were chosen more than 40% of the time were included in the regression model [19]. The second step consists of the development of a linear mixed-effect model with a random split of the data in 70%/30% of train/test set. Specifically, the patient ID was taken as grouping variable. In addition, the random split was repeated 20 times and each model was developed on the train set. The performances were then assessed as *mean absolute error* MAE on the test set, as well as explained variance R^2 both on train and test set (R^2_{train}, R^2_{test}). The results were reported as median(IQR).

III. Results

Figure 1, Table S1, Table S2 and Table S3 show how the different HRV features change according to maturation and the different windowing schemes. Figure 1 displays the following features in function of the PMA: the standard deviation of the *HRV* σ_{RR}, the absolute power in the LF band, the relative $\frac{LF}{LF+VLF}$ power, the Hurst Exponent in the range $[j_1, j_2] = [5, 12]$ $H_{exp_{[j_1,j_2=5,12]}}$ and the width of the singularity spectrum in the same range $C_{2_{[j_1,j_2=5,12]}}$. The left column reports the results for the windowing scheme for the within-bradycardia epochs, while the right one reports the results for the between-bradycardia epochs. The result shows that the power in the LF band and the relative LF power ($\frac{LF}{LF+VLF}$) increase with increasing PMA in both scenarios: in particular, Pearson correlations ρ_{xy} are respectively 72% and 64% for bradycardia epochs, while ρ_{xy} are respectively 71% and 47% for between-bradycardia windows. The post-bradycardia scenario shows 69% for the power in LF band and 37% for $\frac{LF}{LF+VLF}$. Results are here reported for the wavelet approach, but the other spectral methodologies exhibit similar trends (see Tables S1, S2, S3). In addition, the Hurst exponent (derived as the c_1 of the singularity spectrum) decreases with the development (ρ_{xy} are -45% in the bradycardias scenario, -47% in post-bradycardia scenario and -50% in the between-bradycardia scenario), while the width of the singularity spectrum (c_2 parameter) increases with increasing PMA (ρ_{xy} are 54% in the bradycardia scenario, 45% in the post-bradycardia scenario and 43% in the between-bradycardia scenario). The greatest contrast was found with the variability of the heart-rate, σ_{RR}. While the standard deviation increases with infants' maturation in the between-bradycardia epochs, the σ_{RR} does not increase with age within the bradycardic event. Moreover, it is higher in the bradycardia epochs than in the between-bradycardia

scenario ($\rho_{bradycardia} = -4\%$ vs $\rho_{between} = 64\%$ with $p_v = 0.77$ vs $p_v \leq 0.01$). The results are here reported for $f_s = 6\ Hz$ for the temporal and spectral features, while the multifractal parameters are reported for $f_s = 8\ Hz$. The former shows the best regression performances for temporal and spectral features, while the latter was chosen as intermediate frequency of the investigated range for the fractal attributes. A more extended overview of the effect of sampling frequency on the nonlinear features is reported in Table S4. Table II shows how the regression results for the linear mixed-effect model, while Table III reports the features selected by LASSO. Specifically, Table II reports the results for the three different windowing schemes in three different blocks, while the rows report the results for the different feature groups (temporal, spectral and fractal attributes) or all the features combined and for the different sampling frequencies. The different columns respectively report the explained variance in the training set (R^2_{train}), the mean absolute error (MAE) and the explained variance in the test set (R^2_{test}). The feature group (temporal, spectral, fractal and all) have been ranked by the maximal R^2_{train}. Based on the performance of the different models reported in Table II, it is important to observe that:

1) The combination of the spectral and fractal parameters can improve the performance of the LME model, especially in the period between bradycardias (R^2 is higher, while MAE is lower).
2) Temporal features perform poorly in bradycardia epochs (last rows of the third block in Table II).
3) The selected fractal features are mainly in the range $[j_1, j_2] = [5, 12]$. In addition, nonlinear features do not show different regression results with different significant sampling frequencies.

The importance of the regularity parameters in the range $[5, 12]$ is confirmed by Figure 2. The ratios $\frac{VLF}{LF}$ and $\frac{LF}{HF}$ are known to represent sympathovagal balance indices in preterm infants [5] and they should relate to the $Hurst_{exp}$ of the HRV signal [8]. However, Figure 2 shows that the $\frac{VLF}{LF}$ has higher correlation with H_{exp} than $\frac{LF}{HF}$. In addition, the relationship between the spectral ratios and H_{exp} is absent in case of bradycardias.

IV. Discussion

This study provides an overview of autonomic maturation in preterm infants based on heart-rate variability. Based on the pioneering study by Hoyer [12], the current study investigated the maturation of sympathetic and parasympathetic branches with the combination of temporal, spectral and complexity indices. In addition, the effect of bradycardias on the ANS maturation trajectories has been described with three windowing schemes. Three main novel findings can be reported. First, the maturation of infants can be assessed with different spectral and fractal HRV indices with performances that are comparable to the autonomic age model by [12] and EEG-based models [6], [18], [19]. Second, the relationship between the spectral ratio $\frac{VLF}{LF}$ and the Hurst exponent is stronger than the relationship between $\frac{LF}{HF}$ and the Hurst exponent. This might indicate that neonates do not have sympathovagal balance that rely on the typical interplay between LF and HF [1],[8]. Third, the bradycardias can impact HRV maturational features, especially the most common temporal indices that are used in clinical practice.

TABLE I: Overview of all computed features. Besides the first and the second order moments, the table reports all the relative and absolute power features in the frequency domain, namely the power in VLF, LF and HF bands, the ratio between the VLF and LF bands and between LF and HF bands and the normalized LF band power with respect to VLF band and HF band. The spectral features are reported for each PSD estimation approaches that were used in this study. The last section reports the computed multifractal features, i.e. Hurst exponent (H_{exp}) and the (C_2) for the investigated scale ranges: $[j_1, j_2] = [3, 12]$ and $[j_1, j_2] = [5, 12]$.

Temporal features	
Statistical moments	μ_{RR}, σ_{RR}
Spectral features	
Welch	$P(VLF)$,$P(LF)$,$P(HF)$, $\frac{VLF}{LF}$,$\frac{LF}{HF}$,$\frac{LF}{LF+HF}$,$\frac{LF}{LF+VLF}$
SPWVD	$P(VLF)$,$P(LF)$,$P(HF)$, $\frac{VLF}{LF}$,$\frac{LF}{HF}$,$\frac{LF}{LF+HF}$,$\frac{LF}{LF+VLF}$
Wavelet	$P(VLF)$,$P(LF)$,$P(HF)$, $\frac{VLF}{LF}$,$\frac{LF}{HF}$,$\frac{LF}{LF+HF}$,$\frac{LF}{LF+VLF}$
Fractal features	
Multifractality	$H_{exp,[j_1,j_2=\mathbf{5},12]}$, $C_{2,[j_1,j_2=\mathbf{5},12]}$, $H_{exp,[j_1,j_2=3,12]}$,$C_{2,[j_1,j_2=3,12]}$

The different age models that were derived in this study outperform the autonomic age model of [12] ($R^2 = 0.66$) and can be compared to the brain-age model that was derived with EEG data in the same study for both quiet sleep ($R^2 = 0.8$ and $MAE = 1.51\ weeks$) and non-quiet sleep ($R^2 = 0.65$ and $MAE = 1.64\ weeks$) [19]. Figure 1 and Table S1, S2, S3 show that the absolute power in LF and its normalized versions $\frac{LF}{VLF+LF}$, as well as $\frac{LF}{HF+LF}$, grow in all 3 windowing scenarios, which implies that $\frac{VLF}{LF}$ decreases with increasing age, while $\frac{LF}{HF}$ increases. The importance of the spectral features subset is highlighted by the capacity to outperform all other features in age prediction (R^2_{train} in the range [0.57-0.87] and R^2_{test} in the range [0.50-0.62] in Table II) and by the fact that the LF power is selected by LASSO for all the different f_s and with any type of windowing scheme. In addition, the reported autonomic age models show that the tachogram mean μ_{RR} and its standard deviation σ_{RR} increase with maturation, while the regularity measured with the H_{exp} and c_2 decreases.

These findings seem to suggest that the common $LF = [0.05 - 0.15]\ Hz$ is not suitable for infants. Consequently, the ratio $\frac{LF}{HF}$ might not be best suited as index for the sympathovagal balance. David et al. noticed that the fetal heart-rate has such enhanced slow-wave baseline, which increases the power in the VLF band, that both Hoyer et al. and David et al. used the ratio $\frac{VLF}{LF}$ as a possible index to describe the sympatho-vagal interplay [5], [12]. Abry [1] and Doret [8] provided an approach to quantify and understand

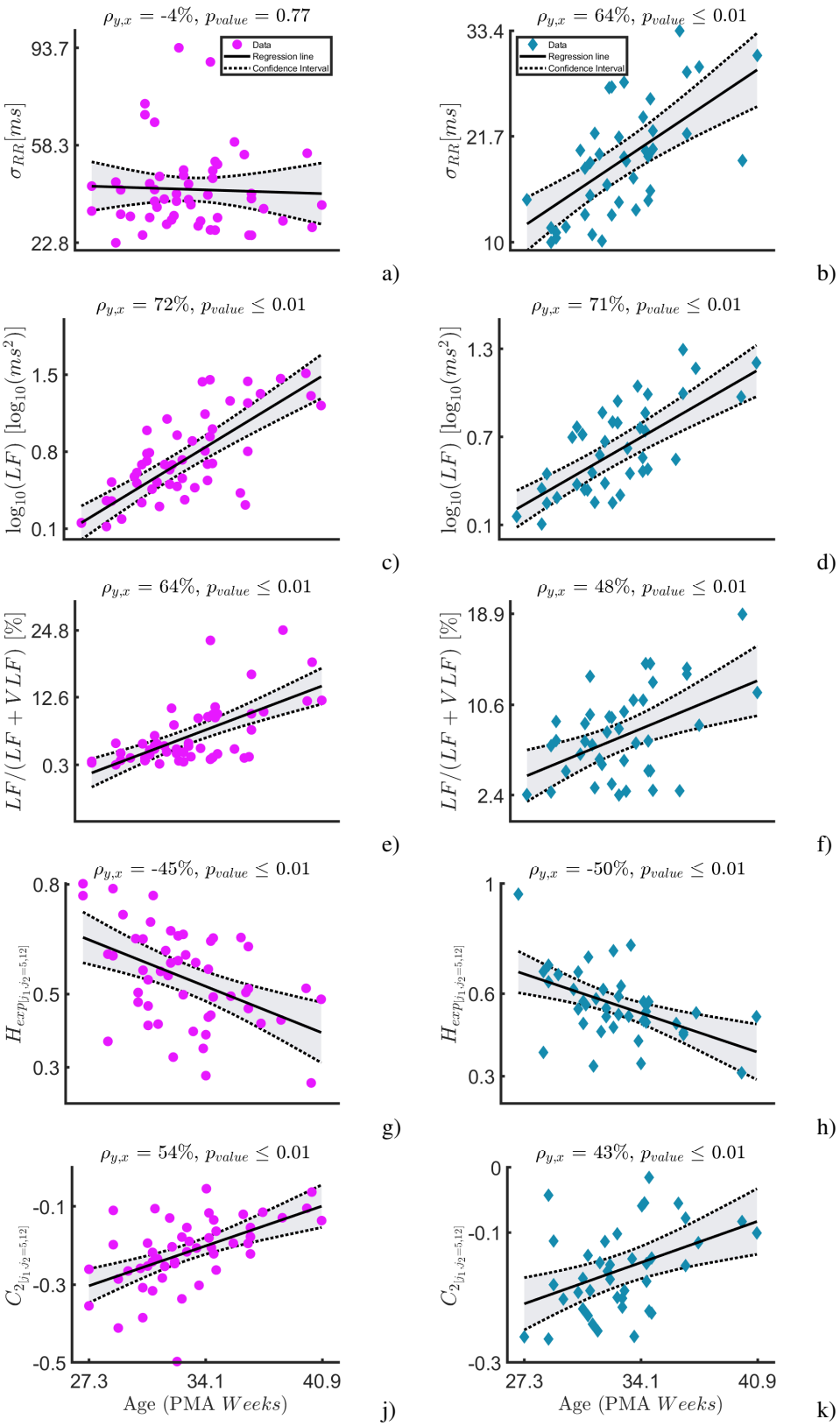


Fig. 1: The figure shows results for the linear-mixed effect regression that models the relationship between HRV features and the post-menstrual age. Specifically, the standard deviation of the tachogram σ_{RR}, the absolute and the relative power in the LF band ($\log_{10}(LF)$ and $\frac{LF}{LF+VLF}$), the Hurst exponent $H_{exp,[j_1,j_2=5,12]}$ and the parameter c_2 are here reported for the sampling frequencies ($f_s = 6\ Hz$,$f_s = 8\ Hz$). The left column (magenta circle data points) reports the result for the bradycardia epochs, while the right column (indigo diamonds data points) reports the result for the between-bradycardia epochs. ρ is the correlation coefficient of the regression and p_{value} represents the significance of the correlation.

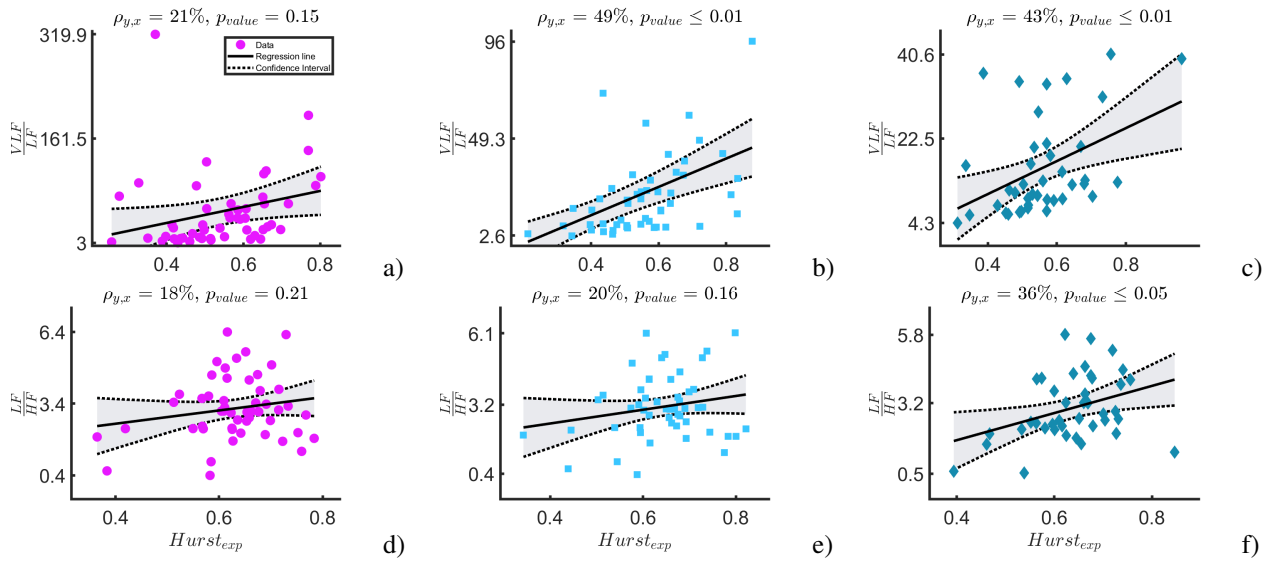


Fig. 2: The figure shows results for the linear-mixed effect regression that models the relationship between $H_{exp,[j_1,j_2=5,12]}$ and $\frac{VLF}{LF}$ in the first row and between $H_{exp,[j_1,j_2=3,12]}$ and $\frac{LF}{HF}$ in the second row. The three columns respectively represents bradycardia epochs (magenta circle data points), post-bradycardia epochs (light-blue squares data points) and between-bradycardia epochs (indigo diamonds data points). ρ is the correlation coefficient of the regression and p_{value} represents the significance of the correlation.

which spectral ratio is actually related to the sympathovagal balance. Based on the assumption that HRV has power-law PSD $\Gamma_X(\nu) = C|\nu|^{-(2H-1)}$, the $\frac{LF}{HF}$ is defined by

$$\frac{LF}{HF} = \frac{\int_{\nu_m}^{\nu_I} \Gamma_X(\nu)d\nu}{\int_{\nu_I}^{\nu_M} \Gamma_X(\nu)d\nu} = \frac{(\nu_I^{2-2H} - \nu_m^{2-2H})}{(\nu_M^{2-2H} - \nu_I^{2-2H})} \tag{11}$$

where $[\nu_m, \nu_I]$,$[\nu_I, \nu_M]$ represent the frequency bands of LF and HF. Equation 11 shows that the higher the Hurst exponent, the higher the $\frac{LF}{HF}$ ratio and, most importantly, the sympathovagal balance is located in the frequency bands where the signals show a fractal or scaling dynamics. Specifically, a higher H_{exp} increases the power of the lower-frequency and the net effect is the increase of the spectral ratio. Therefore, the H_{exp} matches the spectral ratio if its estimation range $[j_1, j_2]$ matches the frequency bands with most of the exponential decay in the PSD. Figure 2 shows the relationship between $\frac{VLF}{LF}$ and $H_{exp,[j_1,j_2=5,12]}$ and the relationship between $\frac{LF}{HF}$ and $H_{exp,[j_1,j_2=3,12]}$. Those panels suggest that the ANS modulation and its fractal regularity lies in the lower-frequency bands, since the $Hurst_{exp}$ is more correlated with spectral parameters (ρ_{xy} between $\frac{VLF}{LF}$ and H are respectively 21%,49%,43% according to different windowing schemes). Those results are in line with Doret [8], who has shown that a redefinition of $\frac{LF}{HF}$ with an extension of bands from the most common adults' range to $LF = [0.02 - 0.15]$ Hz and $HF = [0.15 - 1.3]$ Hz, can discriminate acidosis in fetuses much better. Moreover, those results are in line with the feature selection in Table III, which shows a tendency to select multifractal parameters in the range $[j_1, j_2 = 5, 12]$.

However, the results also highlight the disruptive role of bradycardias in maturation analysis. Gee et al. [10] observed that the LF power, the variance and the regularity of the heart-rate increase before bradycardias. The results in figure 1 and Tables S1, S2, S3 support this increase in variance and regularity (as can be easily noticed by the yaxis of σ_{RR} or any other features of the left column in Figure 1). Moreover, the relationship between the temporal features and maturation is lost, as also reported by the poor R^2 in the last block of Table II. This finding clearly implies that exclusion of bradycardias is fundamental whenever the standard deviation and the mean of the tachogram assess the maturation of ANS. Figure 2 also shows that bradycardias annihilate the expected relationship between the spectral ratios and the Hurst exponent. This is a further proof that bradycardias are a disregulation of the vagal tone [25], which can distort the PSD power-law in Equation 11. However, table II shows that the autonomic age models within bradycardia can maintain comparable performance to the other two windowing schemes thanks to the spectral features. Table III confirms that the most selected power attribute is the power in the band $LF = [0.08 - 0.2]$ Hz, which follows the definition by [10], [5], [12], as further proof of the central role of this range in the bradycardic event and ANS maturation.

Eventually, it is important to highlight the effect of the sampling frequency and the different approaches. Bolea have shown a linear increasing trend for indices such as *Sample Entropy* with increasing mean heart-rate [4]. Based on their results, Bolea et al. concluded that a sampling frequency correction of the indices is needed to capture cardiovascular differences in experiments such as body position changes [4]. However, our study seems to show mild differences in term of regression results. Spectral indices show slight better performance with $f_s = 6$ Hz due to a faster baseline heart-rate of the infant, which implies a higher Nyquist

TABLE II: Linear mixed-effect model performances. For each feature sets and sampling frequencies f_s, the table shows the median(IQR) over the 20 iterations for R^2_{train} on the train set as well as R^2_{test} and the MAE in weeks on test set. IQR here stands for the difference between 75% and 25% quantiles.

Post-bradycardia epochs			
Feature type $\|_{fs}$	R^2_{train}	$MAE(weeks)$	R^2_{test}
All features $\|_{4Hz}$	0.75(0.12)	1.95(0.33)	0.57(0.15)
All features $\|_{6Hz}$	0.73(0.11)	1.88(0.39)	0.57(0.29)
All features $\|_{8Hz}$	0.75(0.1)	1.85(0.3)	0.56(0.23)
All features $\|_{10Hz}$	0.78(0.14)	1.97(0.42)	0.55(0.19)
All features $\|_{12Hz}$	0.75(0.09)	1.83(0.41)	0.57(0.22)
All features $\|_{20Hz}$	0.77(0.15)	1.93(0.28)	0.44(0.29)
Spectral features $\|_{4Hz}$	0.77(0.1)	2.01(0.32)	0.5(0.3)
Spectral features $\|_{6Hz}$	0.74(0.12)	2.01(0.42)	0.5(0.11)
Temporal features $\|_{4Hz}$	0.52(0.23)	2.21(0.53)	0.38(0.22)
Temporal features $\|_{6Hz}$	0.44(0.28)	2(0.56)	0.35(0.19)
Fractal features $\|_{4Hz}$	0.21(0.24)	2.36(0.44)	0.26(0.32)
Fractal features $\|_{6Hz}$	0.33(0.17)	2.21(0.42)	0.33(0.34)
Fractal features $\|_{8Hz}$	0.35(0.13)	2.31(0.54)	0.21(0.22)
Fractal features $\|_{10Hz}$	0.31(0.21)	2.16(0.68)	0.31(0.41)
Fractal features $\|_{12Hz}$	0.26(0.1)	2.18(0.46)	0.43(0.28)
Fractal features $\|_{20Hz}$	0.56(0.18)	2.18(0.5)	0.36(0.22)
Between bradycardia epochs			
Feature type $\|_{fs}$	R^2_{train}	$MAE(weeks)$	R^2_{test}
All features $\|_{4Hz}$	0.57(0.13)	1.99(0.23)	0.52(0.21)
All features $\|_{6Hz}$	0.55(0.12)	1.82(0.28)	0.57(0.24)
All features $\|_{8Hz}$	0.6(0.11)	1.81(0.38)	0.55(0.19)
All features $\|_{10Hz}$	0.63(0.13)	1.8(0.24)	0.6(0.3)
All features $\|_{12Hz}$	0.68(0.11)	1.56(0.39)	0.59(0.16)
All features $\|_{20Hz}$	0.73(0.18)	1.88(0.5)	0.54(0.29)
Temporal features $\|_{4Hz}$	0.58(0.26)	1.86(0.39)	0.5(0.18)
Temporal features $\|_{6Hz}$	0.6(0.33)	2.06(0.38)	0.44(0.24)
Spectral features $\|_{4Hz}$	0.57(0.15)	1.88(0.5)	0.51(0.21)
Spectral features $\|_{6Hz}$	0.59(0.19)	1.93(0.54)	0.59(0.15)
Fractal features $\|_{4Hz}$	0.37(0.31)	1.96(0.8)	0.25(0.38)
Fractal features $\|_{6Hz}$	0.3(0.22)	2.57(0.43)	0.15(0.19)
Fractal features $\|_{8Hz}$	0.22(0.26)	2(0.25)	0.24(0.36)
Fractal features $\|_{10Hz}$	0.34(0.18)	2.09(0.53)	0.45(0.19)
Fractal features $\|_{12Hz}$	0.34(0.28)	2.16(0.53)	0.18(0.31)
Fractal features $\|_{20Hz}$	0.47(0.19)	2.05(0.44)	0.45(0.34)
Bradycardia epochs			
Feature type $\|_{fs}$	R^2_{train}	$MAE(weeks)$	R^2_{test}
All features $\|_{4Hz}$	0.76(0.13)	2(0.33)	0.49(0.23)
All features $\|_{6Hz}$	0.73(0.1)	1.97(0.42)	0.58(0.25)
All features $\|_{8Hz}$	0.7(0.15)	1.91(0.21)	0.5(0.25)
All features $\|_{10Hz}$	0.74(0.13)	1.85(0.31)	0.53(0.16)
All features $\|_{12Hz}$	0.72(0.15)	1.95(0.33)	0.57(0.24)
All features $\|_{20Hz}$	0.76(0.1)	1.91(0.43)	0.49(0.34)
Spectral features $\|_{4Hz}$	0.76(0.1)	1.9(0.25)	0.55(0.23)
Spectral features $\|_{6Hz}$	0.73(0.17)	1.9(0.21)	0.62(0.21)
Fractal features $\|_{4Hz}$	0.2(0.05)	2.42(0.26)	0.21(0.13)
Fractal features $\|_{6Hz}$	0.33(0.07)	2.16(0.4)	0.23(0.18)
Fractal features $\|_{8Hz}$	0.36(0.13)	2.03(0.56)	0.43(0.22)
Fractal features $\|_{10Hz}$	0.34(0.14)	2.21(0.49)	0.35(0.25)
Fractal features $\|_{12Hz}$	0.4(0.16)	2.13(0.56)	0.29(0.28)
Fractal features $\|_{20Hz}$	0.63(0.1)	1.91(0.42)	0.47(0.21)
Temporal features $\|_{4Hz}$	0.1(0.08)	2.57(0.49)	0.1(0.17)
Temporal features $\|_{6Hz}$	0.14(0.1)	2.79(0.35)	0.13(0.13)

frequency. The multifractal indices show an increasing trend with higher f_s (Table S4), but substantial differences are not noticed in the regression results. Therefore, one might choose a sampling frequency to cover the entire band of the tachogram of interests, but the sampling frequency do not have an impact comparable to the bradycardia or the choice of the frequency bands. Although greater care is always suggested in the application of nonlinear indices, the multifractal indices have been revealed to be stable indices to describe the increasing complexity of the ANS. In addition, the different spectral methods (Welch, Wavelet and Wigner-Ville) show very similar spectral trends, but LASSO tends to select time-frequency distribution features (Wavelet and Wigner-Ville, Table S1, S2, S3). This finding supports once more that the bradycardic event and the low-frequency baseline of the neonatal HRV are the most important factors to take into account.

V. Conclusion

The present study investigated ANS maturation by means of temporal, spectral and fractal features of HRV. Three main findings can be reported. First, infants' maturation can be described by means of multifractal and spectral analysis, which show an increasing trend of LF power as well as decreasing trend of fractal regularity with increasing post-menstrual age. The estimated autonomic regression models show performances up to $R^2 = 0.78$ and $MAE = 1.74$ $weeks$ as best measures, comparable to other models reported by different authors [12], [18], [19], [6]. Second, this predominance of LF and VLF bands as well as lower scales for the multifractal indices suggest that the sympathovagal balance of neonates might not simply be related to the $\frac{LF}{HF}$, but the entire HRV band and the regularity of the tachogram should be included to have better understanding of the ANS maturation. Third, bradycardias might forcefully increase the variance of the heart-rate and disrupt the relationship between autonomic indices and age. Eventually, this approach might give a more comprehensive understanding of postnatal maturation of premature neonates and their possible neurovegetative disorders. This research might be a first step to design and support novel therapies or preventive care to preserve infants' development.

VI. Acknowledgments

Research supported by Bijzonder Onderzoeksfonds KU Leuven (BOF) : C24/15/036 "The effect of perinatal stress on the later outcome in preterm babies", imec sbo funds "Wearablehealth", EU: H2020 MSCA-ITN-2018: 'INtegrating Functional Assessment measures for Neonatal Safeguard (INFANS)', funded by the European Commission under Grant Agreement #813483. This research received funding from the Flemish Government under the "Onderzoeksprogramma Artificiële Intelligentie (AI) Vlaanderen" programme. Mario Lavanga is a SB Ph.D. fellow at Fonds voor Wetenschappelijk Onderzoek (FWO), Vlaanderen, supported by the Flemish government.

TABLE III: LASSO selected features for the linear mixed-effect model. For each feature set the features that have been selected more than 40% of times have been reported. σ_{RR} and μ_{RR} stand for the standard deviation and the mean of HRV. $log_{10}(LF)$, $log_{10}(VLF)$, $\frac{VLF}{LF}$ stand for the absolute power in the LF and VLF bands and the ratio between the two. Results are reported for the Wigner-Ville distribution (SPWD) or the wavelet transform. $H_{exp,[j_2,j_2]}$ and $c_{2,[j_2,j_2]}$ stand for the Hurst exponent and the parameter c_2 in the range $[j_1, j_2]$.

Post-bradycardia epochs				
Feature type $\vert_{fs}$				
Spectral $\vert_{4Hz}$	$\log_{10}(LF)_{SPWVD}$	$\log_{10}(LF)_{Wavelet}$		
Spectral $\vert_{6Hz}$	$\log_{10}(LF)_{SPWVD}$	$\log_{10}(LF)_{Wavelet}$		
Fractal $\vert_{4Hz}$	$H_{exp,[j_1,j_2=3,12]}$	$C_{2,[j_1,j_2=3,12]}$		
Fractal $\vert_{6Hz}$	$C_{2,[j_1,j_2=\mathbf{5},12]}$			
Fractal $\vert_{8Hz}$	$H_{exp,[j_1,j_2=\mathbf{5},12]}$	$C_{2,[j_1,j_2=\mathbf{5},12]}$		
Fractal $\vert_{10Hz}$	$H_{exp,[j_1,j_2=\mathbf{5},12]}$	$C_{2,[j_1,j_2=\mathbf{5},12]}$		
Fractal $\vert_{12Hz}$	$C_{2,[j_1,j_2=\mathbf{5},12]}$			
Fractal $\vert_{20Hz}$	$H_{exp,[j_1,j_2=\mathbf{5},12]}$ $C_{2,[j_1,j_2=\mathbf{5},12]}$	$C_{2,[j_1,j_2=\mathbf{5},12]}$	$H_{exp,[j_1,j_2=3,12]}$	
All $\vert_{4Hz}$	$\log_{10}(LF)_{SPWVD}$	$\log_{10}(LF)_{Wavelet}$		
All $\vert_{6Hz}$	$\log_{10}(LF)_{SPWVD}$ $C_{2,[j_1,j_2=3,12]}$	$\log_{10}(LF)_{Wavelet}$	$C_{2,[j_1,j_2=5,12]}$	
All $\vert_{8Hz}$	$\log_{10}(LF)_{Wavelet}$			
All $\vert_{10Hz}$	$\log_{10}(LF)_{SPWVD}$	$\log_{10}(LF)_{Wavelet}$	$C_{2,[j_1,j_2=\mathbf{5},12]}$	
All $\vert_{12Hz}$	$\log_{10}(LF)_{SPWVD}$	$C_{2,[j_1,j_2=\mathbf{5},12]}$		
All $\vert_{20Hz}$	$\log_{10}(LF)_{SPWVD}$	$\log_{10}(LF)_{Wavelet}$		
Between bradycardia epochs				
Feature type $\vert_{fs}$				
Spectral $\vert_{4Hz}$	$\log_{10}(VLF)_{Wavelet}$	$\log_{10}(LF)_{SPWVD}$		
Spectral $\vert_{6Hz}$	$\log_{10}(LF)_{SPWVD}$			
Fractal $\vert_{4Hz}$	$H_{exp,[j_1,j_2=\mathbf{5},12]}$ $C_{2,[j_1,j_2=3,12]}$	$C_{2,[j_1,j_2=\mathbf{5},12]}$	$H_{exp,[j_1,j_2=3,12]}$	
Fractal $\vert_{6Hz}$	$H_{exp,[j_1,j_2=\mathbf{5},12]}$ $C_{2,[j_1,j_2=3,12]}$	$C_{2,[j_1,j_2=\mathbf{5},12]}$	$H_{exp,[j_1,j_2=3,12]}$	
Fractal $\vert_{8Hz}$	$H_{exp,[j_1,j_2=\mathbf{5},12]}$			
Fractal $\vert_{10Hz}$	$H_{exp,[j_1,j_2=\mathbf{5},12]}$	$C_{2,[j_1,j_2=\mathbf{5},12]}$	$H_{exp,[j_1,j_2=3,12]}$	
Fractal $\vert_{12Hz}$	$C_{2,[j_1,j_2=\mathbf{5},12]}$			
Fractal $\vert_{20Hz}$	$H_{exp,[j_1,j_2=\mathbf{5},12]}$	$C_{2,[j_1,j_2=\mathbf{5},12]}$	$H_{exp,[j_1,j_2=3,12]}$	
All $\vert_{4Hz}$	σ_{RR}	$\log_{10}(VLF)_{Wavelet}$	$\log_{10}(LF)_{SPWVD}$	
All $\vert_{6Hz}$	μ_{RR}	$\log_{10}(LF)_{SPWVD}$		
All $\vert_{8Hz}$	$\log_{10}(LF)_{SPWVD}$			
All $\vert_{10Hz}$	μ_{RR}	$\log_{10}(LF)_{SPWVD}$	$C_{2,[j_1,j_2=\mathbf{5},12]}$	
All $\vert_{12Hz}$	$\log_{10}(VLF)_{Wavelet}$	$\log_{10}(LF)_{SPWVD}$	$C_{2,[j_1,j_2=\mathbf{5},12]}$	
All $\vert_{20Hz}$	μ_{RR} $\log_{10}(LF)_{SPWVD}$	σ_{RR} $C_{2,[j_1,j_2=\mathbf{5},12]}$	$\log_{10}(VLF)_{Wavelet}$	
Bradycardia epochs				
Feature type $\vert_{fs}$				
Spectral $\vert_{4Hz}$	$\log_{10}(LF)_{Wavelet}$	$\frac{VLF}{LF}\vert_{Wavelet}$		
Spectral $\vert_{6Hz}$	$\log_{10}(LF)_{Wavelet}$			
Fractal $\vert_{4Hz}$	$C_{2,[j_1,j_2=3,12]}$			
Fractal $\vert_{6Hz}$	$C_{2,[j_1,j_2=\mathbf{5},12]}$	$C_{2,[j_1,j_2=3,12]}$		
Fractal $\vert_{8Hz}$	$H_{exp,[j_1,j_2=\mathbf{5},12]}$	$C_{2,[j_1,j_2=\mathbf{5},12]}$		
Fractal $\vert_{10Hz}$	$H_{exp,[j_1,j_2=\mathbf{5},12]}$	$C_{2,[j_1,j_2=\mathbf{5},12]}$		
Fractal $\vert_{12Hz}$	$H_{exp,[j_1,j_2=\mathbf{5},12]}$	$C_{2,[j_1,j_2=\mathbf{5},12]}$		
Fractal $\vert_{20Hz}$	$H_{exp,[j_1,j_2=\mathbf{5},12]}$ $C_{2,[j_1,j_2=3,12]}$	$C_{2,[j_1,j_2=\mathbf{5},12]}$	$H_{exp,[j_1,j_2=3,12]}$	
All $\vert_{4Hz}$	$\log_{10}(LF)_{Wavelet}$	$C_{2,[j_1,j_2=3,12]}$		
All $\vert_{6Hz}$	$\log_{10}(LF)_{Wavelet}$	$C_{2,[j_1,j_2=\mathbf{5},12]}$	$C_{2,[j_1,j_2=3,12]}$	
All $\vert_{8Hz}$	$\log_{10}(LF)_{Wavelet}$	$C_{2,[j_1,j_2=\mathbf{5},12]}$		
All $\vert_{10Hz}$	$\log_{10}(LF)_{Wavelet}$	$C_{2,[j_1,j_2=\mathbf{5},12]}$		
All $\vert_{12Hz}$	$\log_{10}(LF)_{Wavelet}$	$C_{2,[j_1,j_2=\mathbf{5},12]}$		
All $\vert_{20Hz}$	$\log_{10}(LF)_{Wavelet}$			

REFERENCES

[1] P. Abry, H. Wendt, S. Jaffard, H. Helgason, P. Goncalvés, E. Pereira, C. Gharib, P. Gaucherand, and M. Doret, "Methodology for multifractal analysis of heart rate variability: From LF/HF ratio to wavelet leaders," in *2010 Annual International Conference of the IEEE Engineering in Medicine and Biology*. IEEE, aug 2010, pp. 106–109. [Online]. Available: http://ieeexplore.ieee.org/document/5626124/

[2] E. Atkinson and A. C. Fenton, "Management of apnoea and bradycardia in neonates," *Paediatrics and Child Health*, vol. 19, no. 12, pp. 550–554, dec 2009. [Online]. Available: https://www.sciencedirect.com/science/article/pii/S1751722209001607?dgcid=raven{_}sd{_}recommender{_}email

[3] G. P. Aylward, "Neurodevelopmental outcomes of infants born prematurely," *Journal of Developmental and Behavioral Pediatrics*, vol. 35, no. 6, pp. 394–407, 2014.

[4] J. Bolea, E. Pueyo, M. Orini, and R. Bailón, "Influence of Heart Rate in Non-linear HRV Indices as a Sampling Rate Effect Evaluated on Supine and Standing," *Frontiers in Physiology*, vol. 7, no. NOV, p. 501, nov 2016. [Online]. Available: https://www.frontiersin.org/article/10.3389/fphys.2016.00501/full

[5] M. David, M. Hirsch, J. Karin, E. Toledo, and S. Akselrod, "An estimate of fetal autonomic state by time-frequency analysis of fetal heart rate variability," *Journal of Applied Physiology*, vol. 102, no. 3, 2007. [Online]. Available: http://jap.physiology.org/content/102/3/1057.long

[6] O. De Wel, M. Lavanga, A. Dorado, K. Jansen, A. Dereymaeker, G. Naulaers, and S. Van Huffel, "Complexity Analysis of Neonatal EEG Using Multiscale Entropy: Applications in Brain Maturation and Sleep Stage Classification," *Entropy*, vol. 19, no. 10, p. 516, sep 2017. [Online]. Available: http://www.mdpi.com/1099-4300/19/10/516

[7] A. Dereymaeker, K. Pillay, J. Vervisch, S. Van Huffel, G. Naulaers, K. Jansen, and M. De Vos, "An Automated Quiet Sleep Detection Approach in Preterm Infants as a Gateway to Assess Brain Maturation," *International Journal of Neural Systems*, vol. 27, no. 06, p. 1750023, sep 2017. [Online]. Available: http://www.ncbi.nlm.nih.gov/pubmed/28460602http://www.worldscientific.com/doi/abs/10.1142/S012906571750023X

[8] M. Doret, J. Spilka, V. Chudáček, P. Gonçalves, P. Abry, and H. Stanley, "Fractal Analysis and Hurst Parameter for Intrapartum Fetal Heart Rate Variability Analysis: A Versatile Alternative to Frequency Bands and LF/HF Ratio," *PLOS ONE*, vol. 10, no. 8, p. e0136661, aug 2015. [Online]. Available: http://dx.plos.org/10.1371/journal.pone.0136661

[9] K. Franke, E. Luders, A. May, M. Wilke, and C. Gaser, "Brain maturation: predicting individual BrainAGE in children and adolescents using structural MRI," *Neuroimage*, vol. 63, no. 3, pp. 1305–1312, 2012.

[10] A. H. Gee, R. Barbieri, D. Paydarfar, and P. Indic, "Predicting Bradycardia in Preterm Infants Using Point Process Analysis of Heart Rate," *IEEE Transactions on Biomedical Engineering*, vol. 64, no. 9, pp. 2300–2308, sep 2017. [Online]. Available: http://ieeexplore.ieee.org/document/7756310/

[11] Guidelines, T. N. American, and Guidelines, "Guidelines Heart rate variability," *European Heart Journal*, vol. 17, pp. 354–381, 1996. [Online]. Available: http://www.mendeley.com/research/guidelines-heart-rate-variability-2/

[12] D. Hoyer, F. Tetschke, S. Jaekel, S. Nowack, O. W. Witte, E. Schleußner, and U. Schneider, "Fetal Functional Brain Age Assessed from Universal Developmental Indices Obtained from Neuro-Vegetative Activity Patterns," *PLoS ONE*, vol. 8, no. 9, pp. 1–8, 2013.

[13] P. C. Ivanov, L. a. Amaral, a. L. Goldberger, S. Havlin, M. G. Rosenblum, Z. R. Struzik, and H. E. Stanley, "Multifractality in human heartbeat dynamics." *Nature*, vol. 399, no. 6735, pp. 461–465, 1999.

[14] K. Javorka, Z. Lehotska, M. Kozar, Z. Uhrikova, B. Kolarovszki, M. Javorka, and M. Zibolen, "Heart Rate Variability in Newborns," *Physiol. Res*, vol. 66, pp. 203–214, 2017. [Online]. Available: www.biomed.cas.cz/physiolres

[15] N. Koolen, A. Dereymaeker, O. Rasanen, K. Jansen, J. Vervisch, V. Matic, M. De Vos, G. Naulaers, S. Van Huffel, and S. Vanhatalo, "Data-driven metric representing the maturation of preterm EEG," in *37th Annual International Conference of the IEEE Engineering in Medicine and Biology Society (EMBC)*. IEEE, 2015, pp. 1492–1495. [Online]. Available: http://ieeexplore.ieee.org/document/7318653/

[16] N. Koolen, A. Dereymaeker, O. Räsänen, K. Jansen, J. Vervisch, V. Matic, G. Naulaers, M. De Vos, S. Van Huffel, and S. Vanhatalo, "Early development of synchrony in cortical activations in the human," *Neuroscience*, vol. 322, pp. 298–307, 2016.

[17] C. Krueger, J. H. van Oostrom, and J. Shuster, "A Longitudinal Description of Heart Rate Variability in 28–34-Week-Old Preterm Infants," *Biological Research For Nursing*, vol. 11, no. 3, pp. 261–268, 2010. [Online]. Available: http://brn.sagepub.com/cgi/doi/10.1177/1099800409341175

[18] M. Lavanga, O. De Wel, A. Caicedo, K. Jansen, A. Dereymaeker, G. Naulaers, and S. Van Huffel, "Monitoring Effective Connectivity in the Preterm Brain: A Graph Approach to Study Maturation," *Complexity*, vol. 2017, 2017.

[19] M. Lavanga, O. D. Wel, A. Caicedo, K. Jansen, A. Dereymaeker,

G. Naulaers, and S. V. Huffel, "A brain-age model for preterm infants based on functional connectivity," *Physiological Measurement*, vol. 39, no. 4, p. 044006, apr 2018.

[20] R. F. Leonarduzzi, G. Schlotthauer, and M. E. Torres, "Wavelet leader based multifractal analysis of heart rate variability during myocardial ischaemia," *2010 Annual International Conference of the IEEE Engineering in Medicine and Biology*, pp. 110–113, 2010. [Online]. Available: http://ieeexplore.ieee.org/lpdocs/epic03/wrapper.htm?arnumber=5626091

[21] J. Moeyersons, M. Amoni, S. V. Huffel, R. Willems, and C. Varon, "R-DECO: An open-source Matlab based graphical user interface for the detection and correction of R-peaks," *bioRxiv*, p. 560706, feb 2019.

[22] M. Orini, R. Bailon, L. T. Mainardi, P. Laguna, and P. Flandrin, "Characterization of dynamic interactions between cardiovascular signals by time-frequency coherence," *IEEE Transactions on Biomedical Engineering*, vol. 59, no. 3, pp. 663–673, mar 2012.

[23] P. Paolillo and S. Picone, "Apnea of prematurity," *Journal of Pediatric and Neonatal Individualized Medicine*, vol. 2, no. 2, 2013. [Online]. Available: https://pdfs.semanticscholar.org/342c/3de77ea682ca0dd6ba218d207da850c15e6d.pdf

[24] D. Popivanov, V. Stomonyakov, Z. Minchev, S. Jivkova, P. Dojnov, S. Jivkov, E. Christova, and S. Kosev, "Multifractality of decomposed EEG during imaginary and real visual-motor tracking," *Biological Cybernetics*, vol. 94, no. 2, pp. 149–156, 2006.

[25] S. W. Porges, "Orienting in a defensive world: Mammalian modifications of our evolutionary heritage. A Polyvagal Theory," *Psychophysiology*, vol. 32, no. 4, pp. 301–318, jul 1995. [Online]. Available: http://doi.wiley.com/10.1111/j.1469-8986.1995.tb01213.x

[26] S. L. Smith, S. Haley, H. Slater, and L. J. Moyer-Mileur, "Heart rate variability during caregiving and sleep after massage therapy in preterm infants," *Early Human Development*, vol. 89, no. 8, pp. 525–529, 2013.

[27] H. Wendt, P. Abry, and S. Jaffard, "Bootstrap for Multifractal Analysis," *IEEE Signal Processing Magazine*, vol. 24, no. 4, pp. 38–48, 2007. [Online]. Available: http://ieeexplore.ieee.org/xpl/articleDetails.jsp?arnumber=4286563

[28] D. Widjaja, M. Orini, E. Vlemincx, and S. V. Huffel, "Cardiorespiratory Dynamic Response to Mental Stress: A Multivariate Time-Frequency Analysis," *Computational and Mathematical Methods in Medicine*, 2013. [Online]. Available: http://dx.doi.org/10.1155/2013/451857

TABLE S1: The main temporal, spectral and fractal features are reported for the post-bradycardia periods. The results are reported as median(IQR). IQR stands for *interquartile range*. The temporal and spectral indices are reported for $f_s = 6\ Hz$ and the fractal index is reported for $f_s = 8\ Hz$. The symbol ρ stands for the Pearson correlation coefficient. The symbol ** represents a significant correlation with $p \leq 0.01$, and * is used for a significant correlation with $p \leq 0.05$. $^{n.s.}$ is used to indicate a non-significant correlation.

Median(IQR) - PMA weeks	≤ 32	$(32-36]$	>36	$\rho(\%)$
Temporal features in the POST-bradycardia group, $f_s = 6,\ Hz$				
μ_{RR}	374.65(366.38-391.36)	377.07(364.33-393.69)	387.2(374.98-416.44)	0.39^{**}
σ_{RR}	16.71(12.02-22.05)	25.5(21.65-31.1)	28.47(24.03-32.08)	0.49^{**}
Spectral features in the POST-bradycardia group, $f_s = 6,\ Hz$				
$P(VLF)_{Welch}$	106.24(63.14-156.22)	250.27(180.65-408.05)	287.59(219.04-454.15)	0.38^{**}
$P(VLF)_{SPWD}$	643.16(434.61-1029.4)	1787.69(1081.86-2475.95)	2013.8(1252.61-2653.49)	0.39^{**}
$P(VLF)_{Wavelet}$	36.25(19.22-56.58)	82.2(46.77-119.8)	89.58(62.29-139.78)	0.34^{*}
$P(LF)_{Welch}$	10.91(5.35-16.13)	28.98(13.41-48.24)	50.5(19.82-67.56)	0.63^{**}
$P(LF)_{SPWD}$	70.65(29-94.04)	141.99(84.7-219.13)	450.23(119.78-574.82)	0.69^{**}
$P(LF)_{Wavelet}$	2.14(0.96-3.68)	4.17(2.16-8.9)	17.74(4.94-25.51)	0.69^{**}
$P(HF)_{Welch}$	7.85(3.88-9.53)	9.99(6.08-13.7)	11.84(9.28-24.15)	$0.22^{n.s.}$
$P(HF)_{SPWD}$	38.05(22.98-68.8)	76.75(42.2-106.64)	124.07(87.74-210.87)	0.39^{**}
$P(HF)_{Wavelet}$	0.69(0.36-1.3)	1.61(0.67-2.28)	3.57(1.55-6.4)	0.61^{**}
$\frac{VLF}{LF}_{Welch}$	12.22(7.92-24.59)	9.9(5.8-18.72)	5.45(4.72-8.03)	$0.06^{n.s.}$
$\frac{VLF}{LF}_{SPWD}$	10.76(7.7-13.27)	7.68(4.98-15.57)	4.5(3.11-4.82)	$-0.08^{n.s.}$
$\frac{VLF}{LF}_{Wavelet}$	20.17(12.68-34.29)	19.6(7.22-26.37)	6.98(4.53-10.08)	-0.36^{**}
$\frac{LF}{HF}_{Welch}$	1.47(1.05-1.96)	2.33(1.54-3.36)	3.91(1.9-4.94)	0.56^{**}
$\frac{LF}{HF}_{SPWD}$	1.38(1.14-1.79)	1.91(1.71-2.74)	3.2(1.46-3.81)	0.57^{**}
$\frac{LF}{HF}_{wavelet}$	2.27(1.87-3.02)	3.2(2.76-3.75)	4.56(3.04-5.24)	0.48^{**}
$\frac{LF}{LF+HF}_{Welch}$	59.45(48.87-65.64)	69.97(60.1-76.75)	79.55(65.51-83.17)	0.45^{**}
$\frac{LF}{LF+HF}_{SPWD}$	57.89(53.12-63.96)	65.63(63.1-73.15)	76.13(59.34-79.22)	0.48^{**}
$\frac{LF}{LF+HF}_{Wavelet}$	69.44(65.16-74.67)	76.18(73.35-78.44)	81.96(75.27-83.65)	0.37^{**}
$\frac{LF}{LF+VLF}_{Welch}$	9.11(5.32-12.28)	9.17(5.2-15.27)	15.99(13.78-17.47)	0.48^{**}
$\frac{LF}{LF+VLF}_{SPWD}$	9.14(7.5-11.74)	11.53(6.04-16.74)	19.79(17.18-21.91)	0.56^{**}
$\frac{LF}{LF+VLF}_{Wavelet}$	5.38(3.45-8.7)	4.9(3.67-12.17)	14.06(11.77-18.09)	0.57^{**}
Fractal features in the POST-bradycardia group, $f_s = 8,\ Hz$				
$H_{exp,[j_1,j_2=5,12]}$	0.61(0.52-0.7)	0.55(0.45-0.59)	0.5(0.44-0.56)	-0.47^{**}
$C_{2,[j_1,j_2=5,12]}$	-0.2(-0.26–0.17)	-0.19(-0.21–0.13)	-0.14(-0.15–0.11)	0.45^{**}
$H_{exp,[j_1,j_2=3,12]}$	0.67(0.6-0.71)	0.66(0.59-0.69)	0.62(0.58-0.65)	-0.33^{*}
$C_{2,[j_1,j_2=3,12]}$	-0.14(-0.16–0.1)	-0.11(-0.14–0.08)	-0.09(-0.11–0.09)	$0.2^{n.s.}$

TABLE S2: The main temporal, spectral and fractal features are reported for the BETWEEN-bradycardias periods. The results are reported as median(IQR). IQR stands for *interquartile range*. The temporal and spectral indices are reported for $f_s = 6\ Hz$ and the fractal index is reported for $f_s = 8\ Hz$. The symbol ρ stands for the Pearson correlation coefficient. The symbol ** represents a significant correlation with $p \leq 0.01$, and * is used for a significant correlation with $p \leq 0.05$. $^{n.s.}$ is used to indicate a non-significant correlation.

Temporal features in the BETWEEN-bradycardia group, $f_s = 6$, Hz				
Median(IQR) - PMA weeks	≤ 32	$(32 - 36]$	> 36	$\rho(\%)$
Fractal features in the three age groups				
μ_{RR}	370.51(359.96-388.36)	377.42(363.11-389.25)	394.93(370.01-427.45)	0.47**
σ_{RR}	13.89(10.97-18.49)	19.81(15.72-23.82)	29.1(21.99-30.66)	0.64**
Spectral features in the BETWEEN-bradycardia group, $f_s = 6$, Hz				
$P(VLF)_{Welch}$	68.99(46.83-128.31)	156.67(100.26-217.63)	320.47(184.27-388.76)	0.54**
$P(VLF)_{SPWD}$	358.71(321.19-673.85)	991.87(498.71-1346.25)	2332.8(901.57-2915.13)	0.58**
$P(VLF)_{Wavelet}$	19.23(16.42-40.32)	58.93(35.74-75.05)	108(55.74-147.03)	0.63**
$P(LF)_{Welch}$	8.27(3.78-13.34)	14.99(5.95-25.28)	35.69(26.87-49.37)	0.66**
$P(LF)_{SPWD}$	46.5(25.63-88.72)	106.67(56.24-154.71)	273.11(213.86-373.31)	0.73**
$P(LF)_{Wavelet}$	1.3(0.86-3.38)	4.23(1.93-6.28)	11.34(8.4-15)	0.71**
$P(HF)_{Welch}$	4.85(3.47-6.9)	5.2(4.06-8.12)	11.55(6.11-13.56)	0.17$^{n.s.}$
$P(HF)_{SPWD}$	24.07(19.35-49.89)	50.8(25.85-85.57)	103.73(63.59-129.27)	0.24$^{n.s.}$
$P(HF)_{Wavelet}$	0.45(0.36-1.06)	0.91(0.53-2.2)	2.79(2.09-4.65)	0.62**
$\frac{VLF}{LF}_{Welch}$	9.4(7.9-13.65)	9.22(5.58-18.69)	5.29(4.7-8.4)	-0.2$^{n.s.}$
$\frac{VLF}{LF}_{SPWD}$	7.86(6.19-10.78)	7.5(5.3-13.48)	4.02(3.45-6.87)	-0.14$^{n.s.}$
$\frac{VLF}{LF}_{Wavelet}$	13.42(10.75-19.77)	11.73(8.1-21.36)	7(6.17-10.44)	-0.3$^{n.s.}$
$\frac{HF}{LF}_{Welch}$	1.42(0.75-2.16)	2.19(1.8-3.09)	3.78(2.39-4.23)	0.57**
$\frac{HF}{LF}_{SPWD}$	1.45(0.98-1.6)	1.87(1.61-2.18)	2.8(1.61-3.25)	0.52**
$\frac{HF}{LF}_{Wavelet}$	2.32(1.8-2.84)	3.2(2.39-4.11)	3.67(2.47-4.6)	0.33*
$\frac{LF+HF}{LF}_{Welch}$	58.67(42.64-67.61)	68.69(64.25-75.48)	78.97(70.53-80.88)	0.56**
$\frac{LF+HF}{LF}_{SPWD}$	59.11(49.57-61.62)	65.19(61.76-68.51)	73.67(61.65-76.48)	0.47**
$\frac{LF+HF}{LF}_{Wavelet}$	69.86(64.13-73.93)	76.21(70.43-80.43)	78.39(71.21-82.13)	0.33*
$\frac{LF+VLF}{LF}_{Welch}$	9.71(6.91-11.29)	9.87(5.18-15.21)	16.08(10.77-17.58)	0.42**
$\frac{LF+VLF}{LF}_{SPWD}$	11.29(8.24-13.6)	11.67(6.91-15.29)	19.55(12.12-21.93)	0.44**
$\frac{LF+VLF}{LF}_{Wavelet}$	6.93(4.89-8.53)	7.9(4.63-11.05)	12.57(8.75-13.95)	0.48**
Fractal features in the BETWEEN-bradycardia group, $f_s = 8$, Hz				
$H_{exp,[j_1,j_2=5,12]}$	0.6(0.52-0.68)	0.54(0.5-0.59)	0.48(0.45-0.52)	-0.5**
$C_{2,[j_1,j_2=5,12]}$	-0.19(-0.23–0.14)	-0.17(-0.2–0.14)	-0.09(-0.12–0.08)	0.43**
$H_{exp,[j_1,j_2=3,12]}$	0.68(0.61-0.73)	0.65(0.6-0.67)	0.6(0.55-0.62)	-0.36*
$C_{2,[j_1,j_2=3,12]}$	-0.12(-0.15–0.1)	-0.12(-0.14–0.1)	-0.08(-0.09–0.05)	0.23$^{n.s.}$

TABLE S3: The main temporal, spectral and fractal features are reported for the BRADYCARDIA periods. The results are reported as median(IQR). IQR stands for *interquartile range*. The temporal and spectral indices are reported for $f_s = 6\ Hz$ and the fractal index is reported for $f_s = 8\ Hz$. The symbol ρ stands for the Pearson correlation coefficient. The symbol ** represents a significant correlation with $p \leq 0.01$, and * is used for a significant correlation with $p \leq 0.05$. $^{n.s.}$ is used to indicate a non-significant correlation.

Temporal features in the BRADYCARDIA group, $f_s = 6$, Hz				
Median(IQR) - PMA weeks	≤ 32	$(32 - 36]$	> 36	$\rho(\%)$
Fractal features in the three age groups				
μ_{RR}	384.9(369.62-398.91)	384.16(369.2-397.51)	389.12(377.65-425.8)	0.37**
σ_{RR}	38.31(32.22-44.62)	40.61(32.5-49.81)	35.89(28.43-40.74)	-0.04$^{n.s.}$
Spectral features in the BRADYCARDIA group, $f_s = 6$, Hz				
$P(VLF)_{Welch}$	167.75(101.36-282.21)	312.85(213.81-435.07)	300.05(226.89-457.86)	0.28*
$P(VLF)_{SPWD}$	1109.26(838.07-1615.84)	2025.93(1381.79-3909.12)	2168.01(1229.65-3824.98)	0.31*
$P(VLF)_{Wavelet}$	82.66(46.46-169.3)	122.69(69.22-230.91)	128.03(77.63-164.54)	0.1$^{n.s.}$
$P(LF)_{Welch}$	13(6.4-18.71)	31.09(15.62-52.49)	49.95(20.66-73.54)	0.59**
$P(LF)_{SPWD}$	102.62(68.87-185.63)	216.65(136.5-351.6)	502.28(152.3-734.74)	0.65**
$P(LF)_{Wavelet}$	2.3(1.12-4.03)	4.68(2.8-9.86)	18.66(5.35-26.46)	0.69**
$P(HF)_{Welch}$	7.73(4.31-10.01)	10.63(7.49-14.56)	12.21(9.75-25.52)	0.19$^{n.s.}$
$P(HF)_{SPWD}$	78.85(56.13-117.78)	106.08(78.08-182.35)	148.54(118.65-225.94)	0.3*
$P(HF)_{Wavelet}$	0.6(0.4-1.34)	1.49(0.74-2.57)	3.75(1.58-6.34)	0.59**
$\frac{VLF}{LF}_{Welch}$	13.25(9.99-25.23)	9.86(5.99-19.16)	5.62(4.53-7.99)	0.01$^{n.s.}$
$\frac{VLF}{LF}_{SPWD}$	8.3(6.56-12.13)	8.85(4.78-12.81)	4.18(2.93-4.69)	-0.08$^{n.s.}$
$\frac{VLF}{LF}_{Wavelet}$	43.62(24.21-96.77)	30.2(10.15-56.67)	9.21(4.96-13.94)	-0.47**
$\frac{LF}{HF}_{Welch}$	1.59(1.2-2.07)	2.28(1.69-3.51)	3.86(1.85-4.99)	0.52**
$\frac{LF}{HF}_{SPWD}$	1.3(1.19-1.51)	1.8(1.48-2.26)	2.89(1.35-3.25)	0.57**
$\frac{LF}{HF}_{Wavelet}$	2.36(1.89-2.99)	3.23(2.95-3.84)	4.67(3.02-5.3)	0.48**
$\frac{LF}{LF+HF}_{Welch}$	61.12(53.47-66.49)	69.5(62.38-77.32)	79.32(64.9-83.31)	0.41**
$\frac{LF}{LF+HF}_{SPWD}$	56.49(54.27-60.15)	64.06(59.6-69.35)	74.27(57.44-76.58)	0.49**
$\frac{LF}{LF+HF}_{Wavelet}$	70.22(65.4-74.94)	76.37(73.75-78.74)	82.34(75.1-84.11)	0.37**
$\frac{LF}{LF+VLF}_{Welch}$	7.28(4.92-9.1)	9.2(4.99-14.83)	15.38(14.34-18.08)	0.55**
$\frac{LF}{LF+VLF}_{SPWD}$	10.86(8.03-13.38)	10.86(7.2-17.11)	19.63(18.13-23.51)	0.52**
$\frac{LF}{LF+VLF}_{Wavelet}$	2.57(1.13-3.97)	3.34(2.19-8.97)	10.96(6.69-16.78)	0.64**
Fractal features in the BRADYCARDIA group, $f_s = 8$, Hz				
$H_{exp,[j_1,j_2=5,12]}$	0.61(0.49-0.71)	0.55(0.43-0.62)	0.49(0.43-0.52)	-0.45**
$C_{2,[j_1,j_2=5,12]}$	-0.26(-0.3- -0.21)	-0.21(-0.24- -0.17)	-0.13(-0.18- -0.11)	0.54**
$H_{exp,[j_1,j_2=3,12]}$	0.66(0.62-0.71)	0.64(0.58-0.68)	0.61(0.58-0.62)	-0.36**
$C_{2,[j_1,j_2=3,12]}$	-0.15(-0.2- -0.12)	-0.14(-0.17- -0.11)	-0.11(-0.12- -0.09)	0.31*

TABLE S4: The fractal features are reported in three different age categories and for the following sampling frequencies $f_s = [6, 8, 12]\ Hz$. The results are reported as median(IQR) for the between-bradycardia and bradycardia periods. IQR stands for *interquartile range*. The symbol ρ stands for the Pearson correlation coefficient. The symbol ** represents a significant correlation with $p \leq 0.01$, and * is used for a significant correlation with $p \leq 0.05$. $^{n.s.}$ is used to indicate a non-significant correlation.

Median(IQR) - PMA weeks	≤ 32	$(32 - 36]$	> 36	$\rho(\%)$
Fractal features in the between-bradycardia groups fs = 6				
$H_{exp,[j_1,j_2=5,12]}$	0.55(0.45-0.65)	0.52(0.43-0.55)	0.45(0.4-0.48)	-0.43**
$C_{2,[j_1,j_2=5,12]}$	-0.19(-0.24–0.16)	-0.17(-0.2–0.13)	-0.11(-0.12–0.09)	0.52**
$H_{exp,[j_1,j_2=3,12]}$	0.65(0.56-0.69)	0.61(0.57-0.67)	0.55(0.52-0.59)	-0.39*
$C_{2,[j_1,j_2=3,12]}$	-0.15(-0.17–0.12)	-0.13(-0.15–0.1)	-0.08(-0.1–0.06)	0.39*
Fractal features in the between-bradycardia groups fs = 8				
$H_{exp,[j_1,j_2=5,12]}$	0.6(0.52-0.68)	0.54(0.5-0.59)	0.48(0.45-0.52)	-0.5**
c2vlflf Between-B	-0.19(-0.23–0.14)	-0.17(-0.2–0.14)	-0.09(-0.12–0.08)	0.43**
$H_{exp,[j_1,j_2=3,12]}$	0.68(0.61-0.73)	0.65(0.6-0.67)	0.6(0.55-0.62)	-0.36*
c2lfhf Between-B	-0.12(-0.15–0.1)	-0.12(-0.14–0.1)	-0.08(-0.09–0.05)	0.23$^{n.s.}$
Fractal features in the between-bradycardia groups fs = 12				
$H_{exp,[j_1,j_2=5,12]}$	0.62(0.52-0.68)	0.57(0.52-0.63)	0.52(0.48-0.53)	-0.43**
$C_{2,[j_1,j_2=5,12]}$	-0.18(-0.23–0.16)	-0.15(-0.19–0.12)	-0.09(-0.11–0.08)	0.53**
$H_{exp,[j_1,j_2=3,12]}$	0.68(0.6-0.71)	0.64(0.6-0.69)	0.59(0.54-0.64)	-0.31$^{n.s.}$
$C_{2,[j_1,j_2=3,12]}$	-0.12(-0.14–0.11)	-0.11(-0.12–0.1)	-0.08(-0.1–0.06)	0.26$^{n.s.}$

Median(IQR) - PMA weeks	≤ 32	$(32 - 36]$	> 36	$\rho(\%)$
Fractal features in the BRADYCARDIA period, $fs = 6\ Hz$				
$H_{exp,[j_1,j_2=5,12]}$	0.52(0.42-0.7)	0.48(0.39-0.52)	0.43(0.4-0.46)	-0.36**
$C_{2,[j_1,j_2=5,12]}$	-0.23(-0.29–0.2)	-0.21(-0.24–0.17)	-0.14(-0.18–0.12)	0.55**
$H_{exp,[j_1,j_2=3,12]}$	0.62(0.58-0.67)	0.6(0.53-0.63)	0.57(0.5-0.6)	-0.31*
$C_{2,[j_1,j_2=3,12]}$	-0.19(-0.23–0.15)	-0.16(-0.19–0.14)	-0.1(-0.12–0.09)	0.48**
Fractal features in the BRADYCARDIA period, $fs = 8\ Hz$				
$H_{exp,[j_1,j_2=5,12]}$	0.61(0.49-0.71)	0.55(0.43-0.62)	0.49(0.43-0.52)	-0.45**
$C_{2,[j_1,j_2=5,12]}$	-0.26(-0.3–0.21)	-0.21(-0.24–0.17)	-0.13(-0.18–0.11)	0.54**
$H_{exp,[j_1,j_2=3,12]}$	0.66(0.62-0.71)	0.64(0.58-0.68)	0.61(0.58-0.62)	-0.36**
$C_{2,[j_1,j_2=3,12]}$	-0.15(-0.2–0.12)	-0.14(-0.17–0.11)	-0.11(-0.12–0.09)	0.31*
Fractal features in the BRADYCARDIA period, $fs = 12\ Hz$				
$H_{exp,[j_1,j_2=5,12]}$	0.58(0.5-0.68)	0.56(0.5-0.6)	0.5(0.49-0.53)	-0.36**
$C_{2,[j_1,j_2=5,12]}$	-0.22(-0.28–0.19)	-0.19(-0.22–0.17)	-0.12(-0.14–0.1)	0.58**
$H_{exp,[j_1,j_2=3,12]}$	0.64(0.61-0.68)	0.65(0.61-0.68)	0.63(0.6-0.65)	-0.18$^{n.s.}$
$C_{2,[j_1,j_2=3,12]}$	-0.16(-0.18–0.11)	-0.13(-0.16–0.11)	-0.11(-0.11–0.09)	0.32*